Journal of ELECTRONIC MATERIALS, Vol. 43, No. 6, 2014
DOI: 10.1007/s11664-014-3001-0

Optimal Design of Automotive Thermoelectric Air Conditioner (TEAC)

ALAA ATTAR,[1,2,3] HOSUNG LEE,[1] and SEAN WEERA[1]

1.—Department of Mechanical and Aeronautical Engineering, Western Michigan University, Kalamazoo, MI 49008-5343, USA. 2.—Department of Mechanical Engineering, King Abdulaziz University, Rabigh, Saudi Arabia. 3.—e-mail: alaa.m.attar@wmich.edu

The present work is an analytical study of the optimal design of an automotive thermoelectric air conditioner (TEAC) using a new optimal design method with dimensional analysis that has been recently developed by our research group. The optimal design gives not only the optimal current but also the optimal geometry (i.e., the number of thermocouples, the geometric factor, or the hot fluid parameters). The optimal design for the TEAC is carried out with two configurations: air-to-liquid and air-to-air heat exchangers.

Key words: Thermoelectric air conditioner, automotive thermoelectric cooling, thermoelectric automobile application

Nomenclature

Variables

A_e	Cross-sectional area of thermoelement (mm^2)
A_b	Total base area of thermoelectric air conditioner (TEAC) (mm^2)
A_c	Total fin surface area of cold-side heat sink (mm^2)
A_h	Total fin surface area of hot-side heat sink (mm^2)
A_{UC}	Unit cell base area (mm^2)
COP	Coefficient of performance
c_p	Specific heat (J/kg/K)
H	Total height of TEAC (mm)
h	Heat transfer coefficient of fluid ($W/m^2/K$)
I	Electric current (A)
L	Total length of TEAC (mm)
L_c	Unit cell cold-side length (mm)
L_e	Length of thermoelement (mm)
L_h	Unit cell hot-side length (mm)
k	Thermoelement thermal conductivity (W/m/K), $k = k_p + k_n$
n	Number of thermocouples
n_c	Number of fins for the cold-side heat sink
n_h	Number of fins for the hot-side heat sink
N_k	Dimensionless thermal conductance, $N_k = n(A_e k/L_e)/\eta_h h_h A_h$
N_h	Dimensionless convection, $N_h = \eta_c h_c A_c/\eta_h h_h A_h$
N_I	Dimensionless current, $N_I = \alpha I/(A_e k/L_e)$
Q_c	Total cooling power from TEAC (W)
P_{in}	Total input power of TEAC (W)
PD	Power density (W/cm^2)
R	Electrical resistance of a thermocouple (Ω)
Re	Fluid Reynolds number
T_c	Cold-junction temperature (°C)
T_h	Hot-junction temperature (°C)
$T_{\infty c}$	Fluid temperature (°C)
$T_{\infty h}$	Hot fluid temperature (°C)
ΔT	Thermoelectric temperature difference (°C)
$\Delta T_{cooling}$	Cold air temperature inlet–outlet (°C)
t_c	Cold-side air fin thickness
t_h	Hot-side air fin thickness
V_c	Cold fluid volume flow rate (CFM)
V_h	Hot fluid volume flow rate (L/min for liquid) or (CFM for air)
W	Total width of TEAC (mm)
Z	Figure of merit ($1/K$) = $\alpha^2/\rho k$
z_c	Fin spacing for the cold-side air (mm)
z_h	Fin spacing for the hot-side air (mm)

Greek Symbols

α	Seebeck coefficient (V/K), $\alpha = \alpha_p - \alpha_n$
ρ	Electrical resistivity (Ω/cm), $\rho = \rho_p + \rho_n$
η_c	Fin efficiency of cold-side heat sink
η_h	Fin efficiency of hot-side heat sink

Subscripts

c	Cold

(Received June 27, 2013; accepted January 3, 2014; published online January 25, 2014)

e	Thermoelement
h	Hot
p	p-Type element
n	n-Type element
opt.	Optimal quantity
UC	Unit cell
*	Dimensionless

INTRODUCTION

In the USA, an average of 10% of annual vehicle fuel consumption corresponds to the air-conditioning (AC) system to cool the vehicle cabin.[1] The most common refrigerant used in home and automobile AC is R-134a, which does not have the ozone-depleting properties of Freon, but is nevertheless a strong greenhouse gas and will most probably be banned in the near future.[2] In 2009, the US Department of Energy Office of Energy Efficiency and Renewable Energy (EERE) and the California Energy Commission funded a project to improve the AC systems of vehicles by developing a thermoelectric (TE) heating ventilation and air conditioner (HVAC) which would replace the current conventional AC system.[3] Using a thermoelectric air conditioner (TEAC) system instead of a conventional AC system has two main benefits: it will eliminate the need for R-134a and will provide the ability to cool selected zones instead of the entire cabin, which in turn will reduce fuel consumption.[4] Moreover, 73% of vehicle mileage occurs when the driver is the only occupant, and it is estimated that the total cooling power required to cool the zone of a single occupant is around 630 W, while 3.5 kW to 4.5 kW is needed to cool the entire cabin.[3] The goal of this project is to build a TEAC device that could provide single-occupant cooling with coefficient of performance (COP) of 1.3 or higher.[5]

To achieve the required cooling power and COP, optimization of the parameters for the TEAC system is necessary alongside the types of fluid employed at both the hot and cold heat sinks. For the hot-side (waste) fluid, there are many advantages to the use of liquids instead of air; e.g., they have higher heat transfer coefficients, provide higher power density, and produce lower noise during circulation.[6] However, in addition to the risk of coolant leakage, use of liquids adds more weight and size due to their higher density and the need for an additional radiator.[6] Junior et al.[7] compared a thermoelectric liquid–gas heat exchanger system in steady-state and transient simulation models with a conventional automobile HVAC system. For ambient temperatures of 25°C and 30°C, the conventional automobile HVAC system had a cooling capacity five times higher than the thermoelectric HVAC system for the same input power.[7] Wang et al.[8] designed and analyzed an air-to-liquid thermoelectric HVAC system for a passenger vehicle using a numerical model. They also constructed an experiment to validate their model that was able to reach a COP of 1.55 at a cooling power of 1.55 kW with the same air and liquid inlet temperatures of 30°C.[8] The use of the thermal isolation method allowed COP improvement and determination of the fluid and junction temperatures.[8] Raut and Walke[9] constructed and tested a thermoelectric cooler (TEC) system on a small passenger vehicle with the goal of removing 222 W of heat from the cabin. They used six TEC modules (each with maximum cooling power of 48 W) connected electrically in series and sandwiched between two heat sinks. Their results showed that the system was able to reduce the cabin temperature to as low as 4°C.[9] The Ford Motor Company in collaboration with Gentherm presented their design of a TEAC along with a performance curve in the 2012 Directions in Engine-Efficiency and Emissions Research (DEER) Conference.[10] They tested an air-to-liquid TEAC system that was able to reach a COP of 1.3 at an input power of 400 W using a cold air flow rate of 60 CFM. This paper further discusses the details of that design.

Typical thermoelectric systems are usually attached to heat sinks, which greatly impact the performance of the device. As a result, understanding heat sinks and appropriate Nusselt number correlations is important to validate TEAC designs. Lee[11] used an analytical technique to optimize the fin thickness and fin spacing for both fluid flow over a heat sink and fluid flow through a channel. The applied method optimizes the fin thickness for the maximum heat transfer rate after obtaining the optimum fin spacing. Teertstra et al.[12] developed an analytical correlation to calculate the Nusselt number based on flow in a parallel-plate channel and a combination of developing and fully developed flow. After modifying the correlation to consider fin effects, they compared the new correlation with experimental values, showing good agreement. Zhimin and Fah[13] used two correlations to calculate the Nusselt number for microchannel heat sinks for both laminar and turbulent flow. The results for the thermal resistances were then validated against other work.

The review above shows several TEAC designs, but more investigation of the optimum design is needed. Thus, the present work studies optimization of TEAC air-to-liquid and air-to-air systems using the dimensional analysis method developed by Lee.[14] The objective of this work is to optimize the analytical design of an air-to-liquid TEAC based on a design developed by Gentherm.[10] Our focus is to optimize the thermoelectric parameters (i.e., input electrical current and thermoelement geometric ratio). To do this, the input parameters must first be identified. Since not all of the needed input parameters were readily available, several assumptions had to be made. These assumptions were validated by comparing the results from the present analytical model (using the assumptions) with the results from Gentherm. Since the predicted curve shows close agreement with the Gentherm

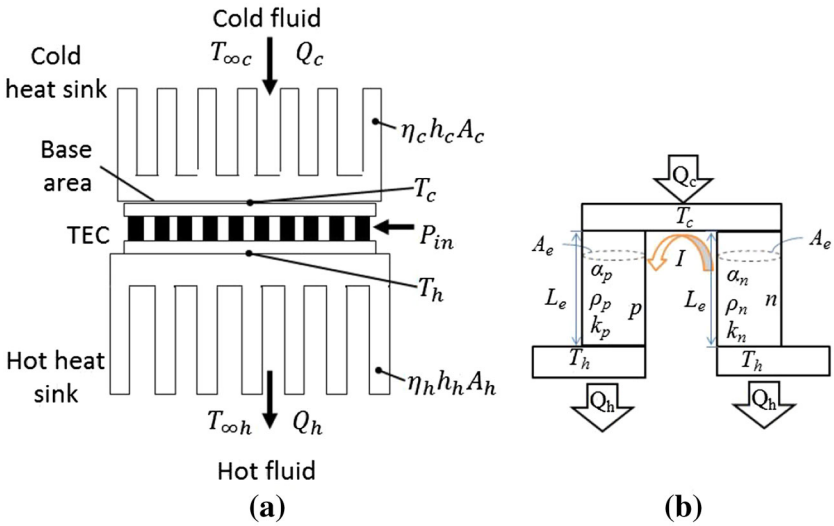

Fig. 1. (a) TEC module with two heat sinks and (b) schematic of a thermoelectric couple.

performance curve, the assumptions and input information can be used as inputs for the optimum design model. Finally, the results from the optimization process are compared against the predicted Gentherm results. Some additional optimization work was done on the air-to-air TEAC to compare its performance with that of an air-to-liquid TEAC.

Optimum Design Background

The dimensional analysis method developed by Lee[14] obtains the maximum cooling power by simultaneously determining the dimensionless current supplied (N_I) and the ratio of the thermal conductance to the convection conductance (N_k) for a given set of fixed parameters. This method converts the four basic heat balance equations (Eqs. 1–4), which are used for a thermoelectric module with heat sinks as shown in Fig. 1a, into two nondimensional equations as shown in Eqs. 5 and 6. Figure 1b shows a schematic of a thermoelectric couple where the p- and n-type pellets have similar height and cross-sectional area.

$$Q_c = \eta_c h_c A_c (T_{\infty c} - T_c), \tag{1}$$

$$Q_c = n\left[\alpha I T_c - \frac{1}{2} I^2 R + \frac{A_e}{L_e} k (T_c - T_h)\right], \tag{2}$$

$$Q_h = n\left[\alpha I T_h + \frac{1}{2} I^2 R + \frac{A_e}{L_e} k (T_c - T_h)\right], \tag{3}$$

$$Q_h = \eta_h h_h A_h (T_h - T_{\infty h}), \tag{4}$$

$$P_{in} = Q_h - Q_c. \tag{5}$$

Q_c and Q_h are the rate of heat transfer for the cold and hot fluids, respectively, P_{in} is the input power, α is the Seebeck coefficient ($\alpha = \alpha_p - \alpha_n$), k is the thermoelement thermal conductivity ($k = k_p + k_n$), R is the electrical resistance of the thermocouple ($R = \frac{L_e}{A_e}(\rho_p + \rho_n)$), and n is the number of thermocouples. It is noted that the thermal resistance of the cold heat sink can be expressed by the reciprocal of the convection conductance $\eta_c h_c A_c$, where η_c is the fin efficiency, h_c is the convection coefficient, and A_c is the total surface area of the cold heat sink.

$$\frac{N_h (T^*_\infty - T^*_c)}{N_k} = N_I T^*_c - \frac{N_I^2}{2 Z T_{\infty h}} + (T^*_c - T^*_h), \tag{6}$$

$$\frac{T^*_h - 1}{N_k} = N_I T^*_h - \frac{N_I^2}{2 Z T_{\infty h}} + (T^*_c - T^*_h). \tag{7}$$

$ZT_{\infty h}$, N_h, N_k, and N_I are defined as the dimensionless figure of merit, convection ratio, the ratio of thermal conductance to convection conductance, and dimensionless current, respectively.

$$ZT_{\infty h} = \frac{\alpha^2}{\rho k} T_{\infty h}, \tag{8}$$

$$N_h = \frac{\eta_c h_c A_c}{\eta_h h_h A_h}, \tag{9}$$

$$N_k = \frac{n (A_e k / L_e)}{\eta_h h_h A_h}, \tag{10}$$

$$N_{\mathrm{I}} = \frac{\alpha I}{A_{\mathrm{e}} k / L_{\mathrm{e}}}. \tag{11}$$

T_{c}^{*}, T_{h}^{*}, and T_{∞}^{*} are the dimensionless cold-junction temperature, the dimensionless hot-junction temperature, and the fluid temperature ratio, respectively, and are defined as

$$T_{\mathrm{c}}^{*} = \frac{T_{\mathrm{c}}}{T_{\infty \mathrm{h}}}, \tag{12}$$

$$T_{\mathrm{h}}^{*} = \frac{T_{\mathrm{h}}}{T_{\infty \mathrm{h}}}, \tag{13}$$

$$T_{\infty}^{*} = \frac{T_{\infty \mathrm{c}}}{T_{\infty \mathrm{h}}}. \tag{14}$$

The dimensionless temperatures are then a function of five independent dimensionless parameters as\

$$T_{\mathrm{c}}^{*} = f(N_{\mathrm{k}}, N_{\mathrm{h}}, N_{\mathrm{I}}, T_{\infty}^{*}, ZT_{\infty \mathrm{h}}), \tag{15}$$

$$T_{\mathrm{h}}^{*} = f(N_{\mathrm{k}}, N_{\mathrm{h}}, N_{\mathrm{I}}, T_{\infty}^{*}, ZT_{\infty \mathrm{h}}). \tag{16}$$

Then, the dimensionless cooling power Q_{c}^{*}, heat rejection Q_{h}^{*}, input power P_{in}^{*}, and COP can be defined as

$$Q_{\mathrm{c}}^{*} = \frac{Q_{\mathrm{c}}}{\eta_{\mathrm{h}} h_{\mathrm{h}} A_{\mathrm{h}} T_{\infty \mathrm{h}}}, \tag{17}$$

$$Q_{\mathrm{h}}^{*} = \frac{Q_{\mathrm{h}}}{\eta_{\mathrm{h}} h_{\mathrm{h}} A_{\mathrm{h}} T_{\infty \mathrm{h}}}, \tag{18}$$

$$P_{\mathrm{in}}^{*} = \frac{P_{\mathrm{in}}}{\eta_{\mathrm{h}} h_{\mathrm{h}} A_{\mathrm{h} T_{\infty \mathrm{h}}}}, \tag{19}$$

$$\mathrm{COP} = \frac{Q_{\mathrm{c}}^{*}}{W_{n}^{*}}. \tag{20}$$

Using these 20 equations, where $ZT_{\infty \mathrm{h}}$, T_{∞}^{*}, and N_{h} are set to be the inputs, the dimensionless parameters N_{k} and N_{I} can be optimized to solve Eqs. 5 and 6 for maximum cooling power.

RESULTS AND DISCUSSION

Air-to-Liquid Study

The objective of this section on the air-to-liquid design study is to re-generate the performance curve provided by Gentherm[10] using the basic ideal equations, readily available data, and several assumptions for information not provided. Figure 2a shows a schematic drawing of the Gentherm design. The system contains two layers of thermoelectric modules having air heat sinks attached to the cold side of each layer and a two-pass liquid heat exchanger sandwiched between the thermoelectric layers in a cross-flow orientation with the air heat sinks. Therefore, the hot side of the thermoelectric modules dissipates heat to the liquid, where the liquid is being cooled independently at a separate radiator. The cold side of the modules cools the incoming air that is directed to the cabin. The dimensions of the prototype were obtained from the work by Gentherm[10] as 300 mm × 120 mm × 50 mm ($W \times L \times H$). Also, the air flow rate was 60 CFM and the cold-side temperature difference between the inlet and exit of cooling air, T_{cooling}, was 16.8°C when the input power P_{in} was 400 W and the COP was 1.3.

Since not all of the needed input parameters were readily available, several assumptions had to be made. Therefore, various initial assumptions were made in order to match Gentherm's performance curve. Some of these assumptions were adjusted until closer predictions were obtained. These assumptions were: the inlet ambient cold temperature $T_{\infty \mathrm{c,in}}$ is 30°C, the inlet hot liquid temperature $T_{\infty \mathrm{h,in}}$ is 30°C, there is a linear change of the cold and hot temperatures along the TEAC system, the liquid (working fluid) is 50% ethylene glycol, the liquid flow rate V_{h} is 7 L per minute, the heat sink and heat exchanger materials are aluminum, the heat sink fin profile length b_{c} is 15 mm, the fin thickness t_{c} is 0.23 mm, the number of fins n_{c} is 437, and the heat exchanger height b_{h} is 5 mm. For the thermoelectric module, the geometry factor (cross-sectional area to length ratio, $A_{\mathrm{e}}/L_{\mathrm{e}}$) G_{e} and the total number of couples n for the system were obtained as approximately 0.365 cm and 880, respectively. Also, all calculations were made under the assumption of steady-state conditions.

To reduce the errors associated with the assumption of neglecting the contact resistances, a technique used by Ahiska and Ahiska[15] was applied to recalculate the material properties of the system. This technique uses the maximum thermoelectric module parameters (typically measurements), which are provided by the manufacturer, to calculate the material properties (i.e., Seebeck coefficient α, electrical resistivity ρ, figure of merit Z, and eventually thermal conductivity k). These reversely calculated material properties result in a somewhat smaller dimensionless figure of merit ($ZT_{\infty \mathrm{h}} = 0.756$)

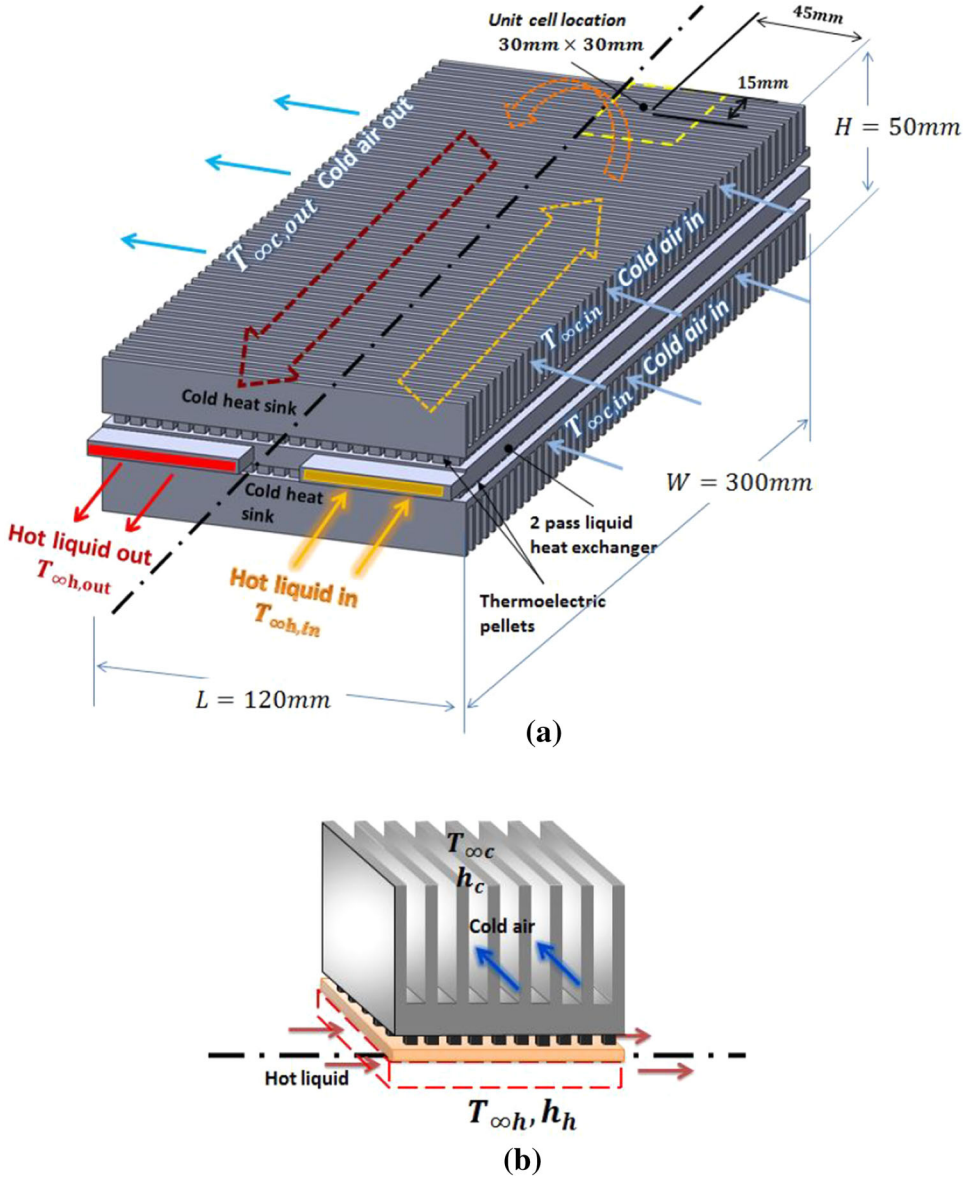

Fig. 2. (a) Schematic diagram of the Gentherm air-to-liquid TEAC and (b) unit cell schematic.

Table I. Comparison between the Gentherm design and the present prediction for two input powers of 400 W and 300 W

Parameter	Gentherm	Prediction	Gentherm	Prediction
P_{in} (W)	400	409.59	300	287.67
I (A)	NA	9.1	NA	7.59
T_c (°C)	NA	18.33	NA	19.05
T_h (°C)	NA	34.93	NA	33.97
$\Delta T_{cooling}$ (°C)	16.8	16.8	15.0	15.0
COP	1.3	1.3	1.6	1.6
Q_c (W)	520	533.02	480	460.13
PD (W/cm^2)	0.722	0.74	0.67	0.64

H = 50 mm, W = 300 mm, L = 120 mm, V_c = 60 CFMAssumptions: V_h = 7.0 L/min, $T_{\infty c,in}$ = 30.0°C, $T_{\infty h,in}$ = 30.0°C, $T_{\infty c}$ = 23.6°C, $T_{\infty h}$ = 31.09°C, t_c = 0.23 mm, n_c = 437, b_c = 15 mm × 2, b_h = 5 mm, A_{UC} = 9.0 cm^2, n = 880, G_e = 0.365 cm, $\alpha_p = -\alpha_n$ = 189.2 μV/K, $\rho_p = \rho_n$ = 0.9 × 10^{-3} Ω/cm, $k_p = k_n$ = 1.6 × 10^{-2} W/cm/K, $ZT_{\infty h}$ = 0.756.

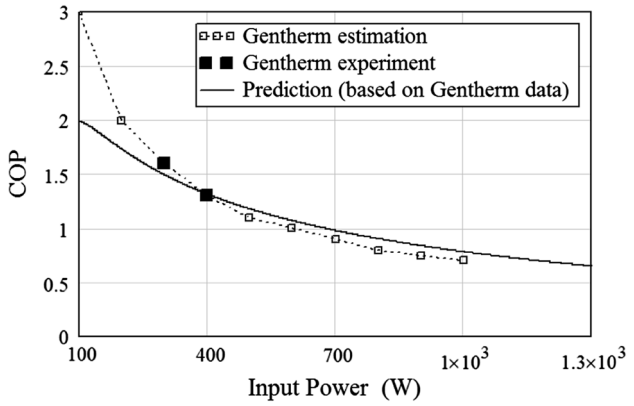

Fig. 3. COP versus input power for Gentherm work and present prediction.

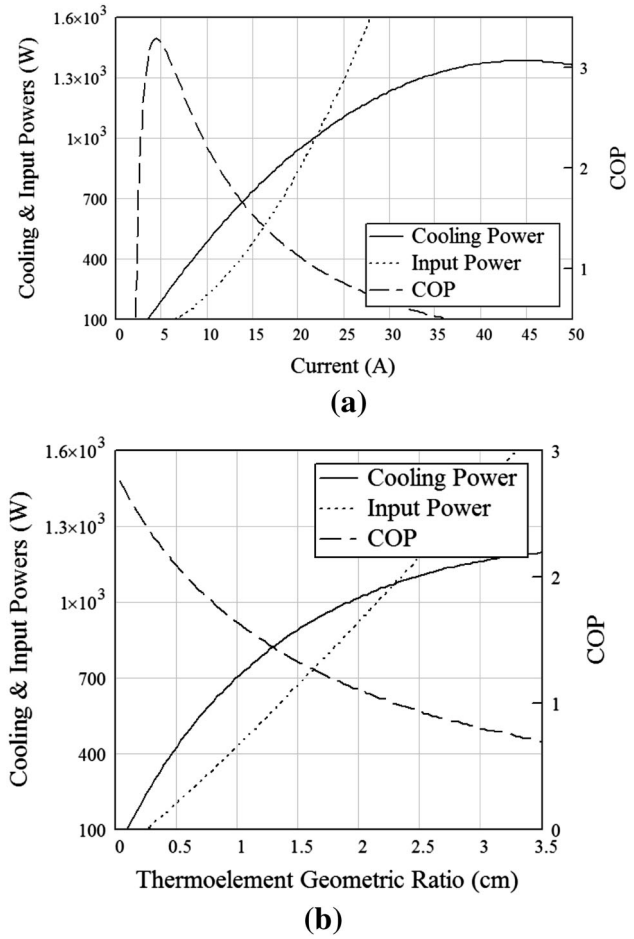

Fig. 4. Cooling power, input power, and COP versus (a) current and (b) geometric ratio G_e.

compared with the figure of merit ($(ZT_{\infty h})_{intrinsic} = 0.815$) based on the original intrinsic material properties. In other words, these material properties are calculated directly from the module, which includes the effect of the contact resistances. Since the material properties of bismuth telluride, in this work, were determined using the same technique of reverse calculation by Ahiska (on a commercial Laird CP10-127-05 module), the material properties and figure of merit themselves include the effect of contact resistances. Thus, there is no need to account for the contact resistances again in the basic equations above.

To simplify the problem, a unit cell of 30 mm × 30 mm base area, as shown in Fig. 2b, is used instead of analyzing the entire system, where the power density of the full scale (cooling power divided by total base area, $A_b = L \times W$) is used to find the unit cell cooling power and input power at the same COP. Gentherm reports that $P_{in} = 400$ W and COP = 1.3, which corresponds to $Q_c = P_{in} \times$ COP = 520 W. The unit cell cooling power $Q_{c,UC}$ is obtained by using the area ratio between the unit cell and the Gentherm TEAC base ($Q_{c,UC} = \frac{1}{2} Q_c \times \frac{A_{UC}}{A_b} = 6.5$ W). A factor of $\frac{1}{2}$ was used because the hot heat sink (liquid) is sandwiched between two cold heat sinks (air). The average cold temperature at the unit cell $T_{\infty c}$ is calculated by using the assumption of a linear change of temperature at the unit cell center where the temperature difference between the cold air inlet and exit $T_{cooling}$ was given. The average hot liquid temperature $T_{\infty h}$ at the unit cell is calculated by using the assumption of a linear change of temperature where the exit hot liquid temperature $T_{\infty h,out}$ is calculated by using the enthalpy flow equation [$Q_h = V_h \rho_h c_{p,h} (T_{\infty h,out} - T_{\infty h,in})$]. The results based on this assumption agree well with temperature calculations from the thermal isolation method found in Ref. 8. The thermal isolation method assumes that the junction temperatures for a unit cell are isolated from the junction temperatures of its neighboring unit cells. Therefore, the junction temperatures of each unit cell are calculated by using the four basic equations, where the unit cell's local ambient temperatures are found from the enthalpy flow equations. The heat sink and heat exchanger parameters are then calculated to match the cooling power and heat rejection of the unit cell by using the Nusselt number correlation found in Ref. 12 for the heat sink and the channel Nusselt number correlation.[11] After that, from the four basic equations, the input current I is varied until Q_c and Q_h match with the unit cell values. Finally, the results were compared with the original data from Gentherm. Table I presents the comparison between Gentherm's provided data and their prediction for two particular experimental data points (at input powers of 400 W and 300 W). Figure 3 shows the COP versus input power for the Gentherm performance curve and the predicted work. From Fig. 3, it can be seen that the experimental data point for COP = 1.3 at $P_{in} = 400$ W matches with the prediction because all the calculations were based on this point. The prediction's trend under a wide range of input power shows fair agreement with the data from Gentherm. This prediction based on Gentherm's data provides a new basis for comparison with the optimum design.

Table II. Comparison between Gentherm predicted design and optimum design

Parameter	Prediction (Gentherm Base)	Optimum design
T_c (°C)	18.33	16.79
T_h (°C)	34.93	35.35
I (A)	9.1	13.66
G_e (cm)	0.365	0.93
P_{in} (W)	409.59	401.22
COP	1.3	1.68
Q_c (W)	533.02	672.38
PD (W/cm^2)	0.74	0.934

V_c = 60.0 CFM, V_h = 7.0 L/min, $T_{\infty c}$ = 23.6°C, $T_{\infty h}$ = 31.09°C, t_c = 0.23 mm, z_c = 0.46 mm, b_c = 15 mm × 2, b_h = 5 mm, h_c = 35.78 W/m^2/K, h_h = 2922 W/m^2/K, $\eta_c \boldsymbol{h}_c \boldsymbol{A}_c$ = 1.28 W/K, $\eta_h \boldsymbol{h}_h \boldsymbol{A}_h$ = 3.07 W/K, N_h = 0.417, A_{UC} = 9.0 cm^2, n = 880, $ZT_{\infty h}$ = 0.756.

Table III. Air-to-liquid optimum design for different ZT values

$ZT_{\infty h}$ = 0.756 (present)	$ZT_{\infty h}$ = 1.0	$ZT_{\infty h}$ = 1.3	$ZT_{\infty h}$ = 2.0
T_c = 16.79°C	T_c = 15.88°C	T_c = 14.96°C	T_c = 13.44°C
T_h = 35.35°C	T_h = 35.95°C	T_h = 36.26°C	T_h = 36.87°C
$G_{e,opt.}$ = 0.93 cm	$G_{e,opt.}$ = 0.84 cm	$G_{e,opt.}$ = 0.75 cm	$G_{e,opt.}$ = 0.61 cm
$I_{opt.}$ = 13.66 A	$I_{opt.}$ = 14.54 A	$I_{opt.}$ = 15.32 A	$I_{opt.}$ = 16.54 A
P_{in} = 401.22 W	P_{in} = 399.26 W	P_{in} = 398.86 W	P_{in} = 400.53 W
$COP_{opt.}$ = 1.68	$COP_{opt.}$ = 1.87	$COP_{opt.}$ = 2.25	$COP_{opt.}$ = 2.61
Q_c = 672.38 W	Q_c = 746.83 W	Q_c = 896.20 W	Q_c = 1046 W
$PD_{opt.}$ = 0.934 W/cm^2	$PD_{opt.}$ = 1.037 W/cm^2	$PD_{opt.}$ = 1.25 W/cm^2	$PD_{opt.}$ = 1.45 W/cm^2

Inputs: $T_{\infty c}$ = 23.55°C, $T_{\infty h}$ = 31.09°C, L = 120 mm, W = 300 mm, A_b = 720 cm^2, H = 50 mm, n = 880, b_c = 15 mm × 2, b_h = 5 mm, V_c = 60 CFM, V_h = 7 L/min, h_c = 35.78 W/m^2/K, h_h = 2922 W/m^2/K, $\eta_c \boldsymbol{h}_c \boldsymbol{A}_c$ = 1.28 W/K, $\eta_h \boldsymbol{h}_h \boldsymbol{A}_h$ = 3.07 W/K, N_h = 0.417.

Air-to-Liquid Optimum Design

The optimization method discussed above requires $ZT_{\infty h}$, T^*_{∞}, and N_h as inputs to obtain all the optimum nondimensional parameters such as N_I, N_k, Q^*_c, COP, T^*_c, T^*_h, and P^*_{in}. These nondimensional parameters can then be converted to the real values using the same thermal resistance of the hot-side heat exchanger ($\eta_h h_h A_h$). As a result, the same thermoelectric material figure of merit and unit cell ambient temperatures ($T_{\infty c}$ and $T_{\infty h}$) that were used for the prediction with Gentherm are used as inputs in the optimum design to obtain $ZT_{\infty h}$ and T^*_{∞}. Also, the same heat sink and heat exchanger parameters are used to obtain N_h.

Figure 4a and b show the cooling power Q_c, input power P_{in}, and COP against the current I and the geometric ratio G_e, respectively. Figure 4a was plotted with N_k = 0.107, while Fig. 4b was plotted with N_I = 0.173. The optimum current for maximum cooling power is different from the optimum current at maximum COP. For the graph of cooling power and COP against geometric ratio, the maximum COP occurs when the cooling power is very small. Using an optimum current halfway between those for maximum cooling power and maximum COP gives a reasonable cooling power and COP without overly compromising one or the other, as indicated in Ref. 14.

A comparison between the prediction based on the Gentherm data and the optimum design for the air-to-liquid TEAC is presented in Table II. The optimum design shows a significant increase in the COP and cooling power due to the optimized current and geometry factor. The optimum design shows an increase of the geometry factor and current when the number of couples is maintained at the same value.

Another advantage of using the dimensionless optimum design method is the ability to set the dimensionless figure of merit $ZT_{\infty h}$ as an input value. The optimized parameters ($G_{e,opt}$ and I_{opt}) of the TEAC are different for different $ZT_{\infty h}$ values. The results in Table III show the inputs and outputs for the optimum design for four different $ZT_{\infty h}$ values for the same input power, inlet cold and hot fluid temperatures, and heat sink and heat exchanger thermal resistances. Different $ZT_{\infty h}$ values result in different optimized parameters ($G_{e,opt}$ and I_{opt}). At $ZT_{\infty h}$ = 2.0, the optimum air-to-liquid TEAC design yields a COP value of about 2.6. Commercial compressor-based air conditioners in automobiles currently have COP values of

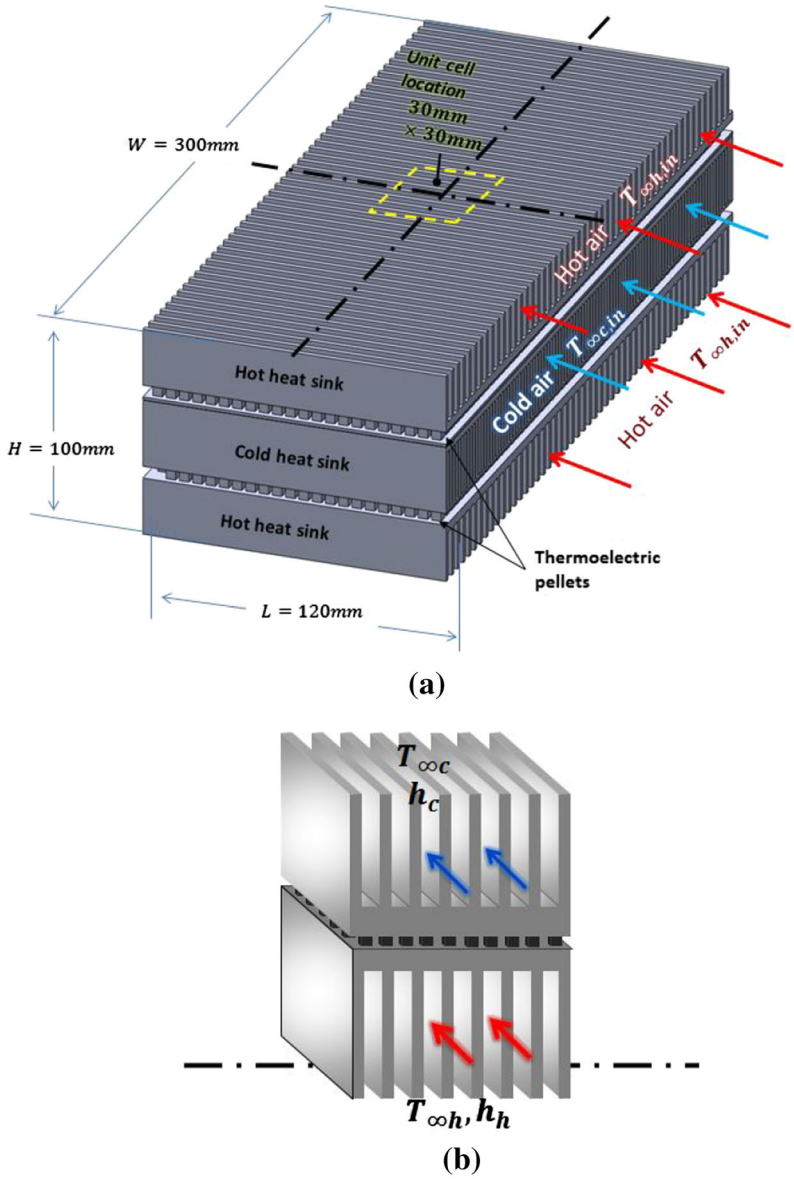

Fig. 5. (a) Schematic of the air-to-air TEAC and (b) unit cell schematic.

Table IV. Results for the air-to-air optimum design compared with the air-to-liquid prediction and air-to-liquid optimum design

Parameter	Air-to-Air Opt. Design	Air-to-Liquid Prediction (Gentherm Base)	Air-to-Liquid Opt. Design
P_{in} (W)	400.45	409.59	401.22
COP	1.3	1.3	1.68
Q_c (W)	520.43	533.02	672.38
PD (W/cm^2)	0.723	0.74	0.934
W (mm) × L (mm)	300 × 120	300 × 120	300 × 120
H (mm)	100	50	50

Air-to-air opt. design parameters: $\boldsymbol{T_{\infty c} = 21.6^{\circ}C}$, $\boldsymbol{T_{\infty h} = 33.57^{\circ}C}$, $\boldsymbol{T_{cooling} = 16.8^{\circ}C}$, $\boldsymbol{T_c = 16.14^{\circ}C}$, $\boldsymbol{T_h = 39.14^{\circ}C}$, $\boldsymbol{A_b = 720\,cm^2}$, $\boldsymbol{A_{UC}}$ = **30 mm × 30 mm**, $\boldsymbol{b_c = 46\,mm}$, t_c = 0.42 mm, t_h = 0.44 mm, z_c = 1.49 mm, z_h = 1.07 mm, $\boldsymbol{b_h = 24\,mm \times 2}$, V_c = 60 CFM, V_h = 120 CFM, $\boldsymbol{Re_c = 474.56}$, $\boldsymbol{Re_h = 677.14}$, Nu_c = 7.25, Nu_h = 7.53, $\boldsymbol{h_c = 67.56\,W/m^2/K}$, $\boldsymbol{h_h = 99.29\,W/m^2/K}$, N_h = 0.58, $\boldsymbol{ZT_{\infty h} = 0.762}$, $\boldsymbol{n_{opt.} = 3662}$, $\boldsymbol{G_e = 0.365\,cm}$, $\boldsymbol{I_{opt.} = 12.9\,A}$.

approximately 2.5. This shows that TEACs, with appropriate materials with $ZT_{\infty h} \approx 2.0$, are highly comparable to conventional compressor-type AC systems used in automobiles.

Air-to-Air Optimum Design

In this section, the air-to-air optimum design is built based on the same base area, cold air flow rate, and input power but with a larger height. In other words, the total height of the air-to-air TEAC was increased in order to match the performance of the prediction based on the Gentherm data. Also, since the heat released is greater while using the same fluid, the design was optimized based on two layers of thermoelectric modules attached to two heat sinks for the hot air. The cold air heat sink is sandwiched between the thermoelectric modules as shown in Fig. 5a. The unit cell for this design, which is shown in Fig. 5b, is located at the center of the TEAC where the unit cell cold fluid temperature, $T_{\infty c}$, and hot fluid temperature, $T_{\infty h}$, are calculated by using the same methods used to calculate the fluid temperatures for the air-to-liquid TEAC. The next step is to optimize the cold and hot heat sink parameters (fin thickness and spacing) in order to maximize $\eta_c h_c A_c$ and $\eta_h h_h A_h$ and to find N_h. The flows through the heat sinks are treated as channel flows, so that the same Nusselt number correlation found in Ref. 13 can be used. Finally, the optimum nondimensional parameters can be obtained. Table IV presents the results obtained for the air-to-air TEAC optimum design when maintaining the input power at 400 W. The performance of the air-to-air TEAC is also compared with the air-to-liquid TEAC prediction and air-to-liquid TEAC optimum design. The results show that, to reach the same performance as the air-to-liquid TEAC prediction based on Gentherm, the total air-to-air TEAC height and hot air flow rate must be doubled.

CONCLUSIONS

The presented work shows that the predicted Gentherm air-to-liquid TEAC design has room for further improvement based on the increased performance for the optimized design. Maintaining the same operating parameters and overall geometry, the optimized air-to-liquid TEAC design shows about 30% improvement in COP compared with the Gentherm design. The optimization procedure manipulates the dimensionless input current N_I and ratio of thermal conductance to convection conductance N_k to observe the effect on the cooling power and COP. In Ref. 14, to simultaneously determine the proper cooling power and COP, halfway between the maximum cooling power and maximum COP was suggested as a good point. For TEAC designs, a justifiable compromise lies somewhere between these two pairs of optimum dimensionless values.

Additionally, the optimum air-to-air TEAC design's COP is comparable to the COP of the air-to-liquid TEAC design at the cost of double the overall height. This demonstrates the versatility of TEAC designs, where air may be used as the hot-side coolant fluid, depending on the constraints of the design.

REFERENCES

1. R. Farrington and J. Rugh, *Impact of Vehicle Air-Conditioning on Fuel Economy, Tailpipe Emissions, and Electric Vehicle Range* (National Renewable Energy Laboratory, 2000), www.nrel.gov/docs/fy00osti/28960.pdf. Accessed 27 June 2013.
2. C.B. Vining, *Nat. Mater.* 6, 83 (2009).
3. J.W. Fairbanks, *Vehicular Thermoelectric Applications Session DEER 2009* (Department of Energy Vehicle Technologies, 2009), http://www1.eere.energy.gov/vehiclesandfuels/pdfs/deer_2009/session7/deer09_fairbanks.pdf. Accessed 27 June 2013.
4. R. Gonzalez, *Automotive Thermoelectric HVAC Development and Demonstration Project*. (California Energy Commission, 2010), http://www.energy.ca.gov/2010publications/CEC-500-2010-FS/CEC-500-2010-FS-018.PDF. Accessed 27 June 2013.
5. C.W. Maranville, *Thermoelectric HVAC and Thermal Comfort Enablers for Light-Duty Vehicle Applications* (Department of Energy Vehicle Technologies, 2012), http://www1.eere.energy.gov/vehiclesandfuels/pdfsmerit_review_2012/adv_combustion/ace047_maranville_2012_o.pdf. Accessed 27 June 2013.
6. T. Barnhart, D. Thomas, and G. Roumayah, *Development of a Thermoelectric Device for an Automotive Zonal HVAC System* (Department of Energy Vehicle Technologies, 2011), https://www1.eere.energy.gov/vehiclesandfuels/pdfs/thermoelectrics_app_2012/tuesday/barnhart.pdf. Accessed 27 June 2013.
7. C.S. Junior, N.C. Strupp, N.C. Lemke, and J. Koehler, *J. Electron. Mater.* (2009). doi:10.1007/s11664-009-0749-8.
8. D. Wang, D. Crane, and J. LaGrandeur, SAE Technical Paper 2010-01-0807 (2010). doi:10.4271/2010-01-0807.
9. M.S. Raut and P.V. Walke, *IJCA Proceedings on International Conference on Emerging Frontiers in Technology for Rural Area* (New York: Foundation of Computer Science, 2012), p. 27.
10. C.W. Maranville, J. Schneider, L. Chaney, T. Barnhart, and J.P. Heremans, *Improving Efficiency of a Vehicle HVAC System with Comfort Modeling, Zonal Design, and Thermoelectric Devices* (DEER Conference, 2012), http://www1.eere.energy.gov/vehiclesandfuels/pdfs/deer_2012/thursday/presentations/deer12_maranville.pdf. Accessed 10 June 2013.
11. H. Lee, *Thermal Design: Heat Sinks, Thermoelectrics, Heat Pipes, Compact Heat Exchangers, and Solar Cells* (Hoboken, NJ: Wiley, 2010).
12. P. Teertstra, M.M. Yovanovich, and J.R. Culham, *Fifteenth Annual IEEE Semiconductor Thermal Measurement and Management Symposium* (1999). doi:10.1109/STHERM.1999.762426.
13. W. Zhimin and C.K. Fah, *Proceedings of the 1st Electronic Packaging Technology Conference* (1997). doi:10.1109/EPTC.1997.723898.
14. H. Lee, *Appl. Energy* 106, 79 (2013).
15. R. Ahiska and K. Ahiska, *Energy Convers. Manag.* 51, 338 (2010).